Stem Cells Trans Med Papers in Press. Published on April 21, 2015 as Manuscript sctm.2014-0209

STEM CELLS TRANSLATIONAL MEDICINE®

CELL-BASED DRUG DEVELOPMENT, SCREENING, AND TOXICOLOGY

DNA Damage Response in Neonatal and Adult Stromal Cells Compared With Induced Pluripotent Stem Cells

STEFANIE LIEDTKE,[a] SOPHIE BIEBERNICK,[a] TEJA FALK RADKE,[a] DANIELA STAPELKAMP,[a] CAROLIN COENEN,[a] HOLM ZAEHRES,[b] GERHARD FRITZ,[c] GESINE KOGLER[a]

Key Words. DNA Repair • DNA damage response • Neonatal and adult stromal cells • MSC • iPSC • Osteogenesis • MNU • Ionizing radiation

[a]Institute for Transplantation Diagnostics and Cell Therapeutics and [c]Institute of Toxicology, Heinrich-Heine-University Medical Center, Düsseldorf, Germany; [b]Department Cell and Developmental Biology, Max Planck Institute for Molecular Biomedicine, Münster, Germany

Correspondence: Gesine Kogler, Ph.D., Institute for Transplantation Diagnostics and Cell Therapeutics, Heinrich-Heine-University Medical Center, Moorenstrasse 5, D-40225 Düsseldorf, Germany. Telephone: 49-211-8104342; E-Mail: gesine.koegler@med.uni-duesseldorf.de

Received September 19, 2014; accepted for publication February 23, 2015.

1066-5099/2015/$20.00/0

http://dx.doi.org/10.5966/sctm.2014-0209

ABSTRACT

Comprehensive analyses comparing individual DNA damage response (DDR) of induced pluripotent stem cells (iPSCs) with neonatal stromal cells with respect to their developmental age are limited. The imperative necessity of providing developmental age-matched cell sources for meaningful toxicological drug safety assessments in replacement of animal-based testing strategies is evident. Here, DDR after radiation or treatment with *N*-methyl-*N*-nitrosurea (MNU) was determined in iPSCs compared with neonatal and bone marrow stromal cells. Neonatal and adult stromal cells showed no significant morphologically detectable cytotoxicity following treatment with 1 Gy or 1 mM MNU, whereas iPSCs revealed a much higher sensitivity. Foci analyses revealed an effective DNA repair in stromal cell types and iPSCs, as reflected by a rapid formation and disappearance of phosphorylated ATM and γH2AX foci. Furthermore, quantitative polymerase chain reaction analyses revealed the highest basic expression level of DDR and repair-associated genes in iPSCs, followed by neonatal stromal cells and adult stromal cells with the lowest expression levels. In addition, the influence of genotoxic stress prior and during osteogenic differentiation of neonatal and adult stromal cells was analyzed applying common differentiation procedures. Experiments presented here suggest a developmental age-dependent basic expression level of genes involved in the processing of DNA damage. In addition a differentiation-dependent downregulation of repair genes was observed during osteogenesis. These results strongly support the requirement to provide adequate cell sources for toxicological in vitro drug testing strategies that match to the developmental age and differentiation status of the presumptive target cell of interest. STEM CELLS TRANSLATIONAL MEDICINE *2015;4:1–14*

SIGNIFICANCE

The results obtained in this study advance the understanding of DNA damage processing in human neonatal stromal cells as compared with adult stromal cells and induced pluripotent stem cells (iPSCs). The data suggest developmental age-dependent differences in DNA damage repair capacity. In iPSCs (closest to embryonic stem cells), the highest expression level of DNA damage response and repair genes was found, followed by neonatal stromal cells and adult stromal cells with the lowest overall expression. In addition, a differentiation-dependent downregulation of repair capacity was observed during osteogenic differentiation in neonatal stromal cells. Notably, the impact of genotoxic stress on osteogenic differentiation depended on the time the genotoxic insult took place and, moreover, was agent-specific. These results strongly support the necessity of offering and establishing adequate cell sources for informative toxicological testing matching to the developmental age and differentiation status of the respective cell of interest.

INTRODUCTION

Cells generally respond to genotoxic stress by activating the DNA damage response (DDR). An orchestrated network of signaling pathways with ATM (ataxia telangiectasia mutated gene) as the central sensor protein leads to phosphorylation of the DDR mediator H2AX (histone family member X) [1]. Phosphorylated γH2AX then triggers a cascade of events leading to the recruitment of various factors, including BRCA1 (breast cancer 1 gene) and TP53 (tumor protein p53) [2, 3]. Finally, other downstream transducer proteins mediate complex responses eventually affecting DNA repair, cell cycle progression, and cell death [2, 4].

Cells can cope with damaged DNA by activating different repair pathways. DNA double-strand breaks (DSBs), which can be induced by radiation and other types of genotoxic noxae or during replication are mainly repaired by homologous recombination (HR) or nonhomologous end joining (NHEJ) [5, 6]. HR is an error-free repair mechanism using sister chromatids as a template for accurate repair of DSBs in somatic mammalian cells [7]. However, NHEJ is an error-prone mechanism involved in the recognition and processing of DNA ends by the Ku70/Ku80 heterodimer complex [8, 9]. Alternative repair of DNA damage, which can arise, for instance, from exposure to alkylating agents, is covered by the base excision repair (BER) [10, 11], nucleotide excision repair (NER) [12, 13] and the mismatch repair (MMR) pathway [14]. It was recently described that cells can evade cellular damage by inducing cellular differentiation programs [15].

Cellular responses to ionizing radiation (IR) have been analyzed in many cell types including induced pluripotent stem cells (iPSCs) [16–20]. For human adult mesenchymal stem cells (MSCs), radioresistance was described, showing that long-term proliferation is comparable with that of known radio-resistant cell types, such as the A594 lung cancer cell line [21–23].

Moreover, a variable anatomic site-dependent response and recovery from irradiation exists, uncovering a skeletal site-specific higher radioresistance in human bone marrow multipotent stromal cell (BM MSC)-derived from orofacial bone [24]. Furthermore, a close link of repair capacity and stem cell differentiation was reviewed for many stem cell types [15]. In general, a highly efficient DNA repair network that becomes less efficient upon differentiation was hypothesized for human stem cells including iPSCs [25]. It is assumed that a high repair capacity of stem cells favors the maintenance of their genomic integrity, which is essential for their function [26].

Most experiments available in the literature analyzing the DNA damage response after radiation were performed with adult BM MSCs [22]. So far, no comprehensive data are available comparing neonatal stromal cells versus neonatal stromal cell-derived iPSCs. iPSCs generated from neonatal unrestricted somatic stromal cells (USSCs) were established and offer an attractive source of neonatal stromal cells for reprogramming [27]. USSCs themselves were previously described in 2004, representing a neonatal counterpart to human adult BM MSCs [28, 29]. Since 2010, distinct neonatal stromal cell populations with multipotent differentiation capacities within cord blood were described, namely USSCs and cord blood multipotent stromal cells (CB MSCs), which can be distinguished by their inherent adipogenic differentiation potential [30, 31] and their *HOX* gene expression profile [32]. Neonatal USSCs can be easily differentiated into the osteogenic and chondrogenic lineage in vitro but can only be differentiated into the adipogenic lineage after coculture with CB MSCs [33]. Detailed characterization of the individual inherent differentiation capacity is available [30, 34–36]. Therefore, neonatal stromal cells (like USSCs) can be assumed to provide favorable features for developmental toxicity testing to assess the potential toxicity of drug candidates and chemicals in the neonatal system [37]. Recently, human iPSCs were considered as an alternative to the established mouse embryonic stem cell test [38]. It is evident that well-characterized in vitro model systems are required for an efficient and meaningful toxicological drug testing—in particular of drugs potentially affecting developmental processes—that circumvents the use of animal testing, thereby promoting the global intended 3R concept (reduction, refinement, and replacement of animal experiments).

The study presented here aims to spot differences in DDR responses of neonatal stromal cells, adult stromal cells, and USSC-derived iPSCs following genotoxic treatment. In order to additionally unravel genotoxin-specific responses, IR was chosen as a prototypical inducer of DNA DSBs and the chemical mutagen *N*-methyl-*N*-nitrosurea (MNU) evoking DNA base damage by alkylation [13]. Moreover, the influence of both types of genotoxins on the osteogenic differentiation capacity of neonatal stromal cells and adult BM MSCs was determined. The results presented in this study highlight the need for more relevant alternative in vitro systems for toxicological testing [39], which take into account the different susceptibility of neonatal and adult stromal cells compared with iPSC.

Materials and Methods

Generation and Expansion of USSCs and BM MSCs

USSCs were generated as described previously [30, 35]. In brief, CB was collected from the umbilical cord vein with informed consent of the mother. Mononuclear cells (MNCs) were obtained by Ficoll (Biochrom AG, Berlin, Germany, http://www.biochrom.de; density 1.077 g/cm^3) gradient separation followed by ammonium chloride lysis of RBCs. 5–7 $\times$ 10^6 CB MNC/ml were cultured in low glucose Dulbecco's modified Eagle's medium (DMEM) (Lonza, Walkersville, MD, http://www.lonza.com) with 30% fetal calf serum (Perbio, Cramlington, U.K., http://www.piercenet.com), 10^{-7} M dexamethasone (Sigma-Aldrich, St. Louis, MO, http://www.sigmaaldrich.com), and penicillin/streptomycin/L-glutamine (PSG; Lonza).

Cells were cultured at 37°C in a humidified atmosphere with 5% CO_2 until reaching 80% confluence. USSCs and BM MSCs were detached with 0.25% trypsin. To evaluate the cumulative population doublings (CPD), the following formula was applied: PD = [log (n1/n0)]/log2 CPD = ΣPD, where n1 is the number harvested cells, and n0 is the number plated cells.

Generation and Expansion of iPSCs

Induced pluripotent stem cells were generated from USSC line (SA8/25(passage(p)3) by retroviral expression of the transcription factors OCT4, KLF4, SOX2, and cMYC as described in the publication by Zaehres et al. [27]. Reprogramming was performed with the vectors described in the original paper by Takahashi et al. [40].

iPSCs were expanded on murine embryonic fibroblasts (MEFs) in serum-free medium consisting of knockout (KO) DMEM supplemented with 20% serum replacement (both Invitrogen, Carlsbad, CA, http://www.invitrogen.com), 1% nonessential amino acids (Sigma-Aldrich), 40 ng/ml basic fibroblast growth factor (100 μg/ml stock solution; Prepotech, Rocky Hill, NJ, https://www.peprotech.com), 2-mercaptoethanol (0.2 μl/ml; Gibco, Grand Island, NY, http://www.invitrogen.com), and 2% PSG (Lonza). Prior to conduction of the experiments, colonies were harvested and cultivated feeder-free for at least two passages on Matrigel (BD Biosciences, San Diego, CA, http://www.bdbiosciences.com) using MEF-conditioned medium (serum-free medium as described above conditioned on MEFs for 48 hours and then mixed 1:1 with fresh medium).

For both serum-free and feeder-free cultivation, culture conditions were 37°C with 5% CO_2 in humidified atmosphere. Respective medium was changed on a daily basis, and harvest was

performed by removal of medium, incubation with collagenase IV (1 mg/ml in KO DMEM; both Invitrogen) for 5 minutes, and gentle aspiration of detached colonies/cells.

In Vitro Differentiation

USSCs were differentiated as described previously [35]. In brief, for osteogenic differentiation induction medium containing sodium L-ascorbate, β-glycerolphosphate disodium salt hydrate, and dexamethasone was applied and changed twice a week over a total runtime of 14 days. To detect mineralization, the differentiated cells were fixed with cold ethanol (70%, 10min) and stained with alizarin red S (Sigma-Aldrich), as well as Von Kossa (5% silver nitrate; Roth, Karlsruhe, Germany, http://www.carlroth.de) according to standard protocols. For quantification of alizarin red, 800 μl of 10% acetic acid were added and incubated for 30 minutes while shaking. The cells were detached with a cell scraper and transferred to a 1.5-ml Eppendorf tube. Samples were vortexed for 30 seconds, then heated at 85°C for 10 minutes, and finally cooled down on ice for 5 minutes. After a centrifugation step at 24,500*g* for 15 minutes, 500 μl of the supernatant were mixed with 200 μl of 10% ammonium hydroxide and measured photometrically in a plate reader (Bio-Tek Instruments Inc., Winooski, VT, http://www.biotek.com) at 405 nm. The values of the respective negative control were subtracted from differentiated cells.

Irradiation Treatment

Exponentially growing cells were irradiated at 37°C with the x-ray device RS225 from Gulmay (Byfleet, U.K., http://www.gulmay.com) with doses of 1–5 Gy, and analyses were performed 1, 6, and 24 hours later. Formation and decline of IR-induced DNA DSBs was monitored by immunocytochemical detection of nuclear *p*-ATM and γH2AX foci as described under Immunocytochemistry below.

Treatment With MNU

Prior to treatment of cultivated cells with MNU (Sigma), cells were washed twice with phosphate-buffered saline (PBS) and incubated for 7 minutes at 37°C. After removal of PBS different concentrations of MNU (stock solution: 1 M in dimethyl sulfoxide [DMSO]) were added to the cells. After treatment for different periods of time, the alkylating agent was removed, and cells were further cultivated as mentioned in the corresponding legends to figures.

Total RNA Extraction and Reverse Transcription

Total RNA was extracted from cell samples at day 0 in a 40-μl volume applying the InviTrap RNA mini kit (Stratec, Birkenfeld, Germany, http://www.stratec.com) according to the manufacturer's instructions. RNA from differentiated (calcified) cells was isolated using the TRI reagent RNA isolation reagent (Sigma-Aldrich) following a standard protocol of a phenol-chloroform extraction. Determination of RNA concentrations and purity was carried out by applying a Nanodrop device (NanoDropTechnologies, Thermo Fisher Scientific, Waltham, MA, http://www.thermofisher.com). After TRIzol isolation, a DNAse digest was performed with RNA samples prior to cDNA synthesis to avoid DNA contamination applying DNAse I amplification grade (Invitrogen) according to the manufacturer's instructions. Reverse transcription was performed for 50 minutes at 55°C using a first-strand cDNA synthesis kit (Invitrogen) and the enclosed oligo$(dT)_{20}$ primer. Up to 1,000 ng of total RNA were converted into first-strand cDNA in a 20-μl reaction. All control reactions provided with this system were carried out to monitor the efficiency of cDNA synthesis. Prior to quantitative polymerase chain reaction (qPCR), the completed first-strand reaction was heat-inactivated at 85°C for at least 10 minutes. Finally, cDNA was treated with RNaseH according to the manufacturer's protocol.

qPCR

PCR was carried out with intron-spanning primers specific for each gene (Thermo Fisher Scientific). The sequences for primers (supplemental online Table 1) were carefully examined and checked for their specificity by applying BLASTn (http://blast.ncbi.nlm.nih.gov/Blast.cgi). *RPL13A* was used as reference gene for normalization because it stays stable during differentiation. qPCR was carried out with SYBR Green PCR Mastermix (Applied Biosystems, Foster City, CA, http://www.appliedbiosystems.com) using 10–50 ng of template cDNA. All reactions were run in triplicate, respectively, on a Step One Plus (Applied Biosystems). PCRs were run in a total volume of 25 μl containing 12.5 μl of Power SYBR Green PCR, 9.5 μl of distilled H_2O, 1 μl of template, and 1 μl (0.2 μM) of each primer. The PCR parameters were as follows: 10 minutes at 95°C for initial denaturation and *Taq* polymerase activation followed by 15 seconds at 95°C and 1 minute at 60°C for 35 cycles. Specificity of the PCR product was confirmed by analyzing the melting curves. To run and analyze the comparative Ct experiments, StepOne software (version 2.1; Applied Biosystems) was used. The threshold was kept at 0.2 for all experiments. Relative changes in gene expression were calculated following the $\Delta\Delta$Ct method with *RPL13A* as internal standard and normalized to native untreated samples. Differential gene expression was calculated by the equation 2^-$\Delta\Delta$Ct, and the untreated control was set to 1. The results are illustrated as mean values (n = 3) with standard deviations.

Immunocytochemistry

Immunocytochemical staining was performed using an antibody against human anti-phosphohistone H2A.X (Ser139) clone JBW301 (1:250; Merck Millipore, Billerica, MA, http://www.millipore.com) and an antibody against ATM (pSer1981) (10H11.E12) (1:1,000; Novus Biologicals, San Diego, CA, http://www.novusbio.com). Secondary antibody (rhodamine red X-conjugated AffiniPure goat anti-mouse IgG; Jackson Immunoresearch Laboratories, West Grove, PA, http://www.jacksonimmuno.com) was applied in a 1:2,000 dilution. All photographs were taken with an Axiocam HRC camera (Carl Zeiss, Jena, Germany, http://www.zeiss.com) under the same parameters carefully defined for each antibody at the Axioplan 2 imaging microscope (Carl Zeiss) with Axiovision software, release 4.8.2 (Zeiss).

The repair kinetics of DNA DSBs were monitored by the formation and removal of γH2AX and *p*-ATM foci (red) in cells counterstained with the nuclear dye 4′,6-diamidino-2-phenylindole (blue). Immunocytochemical analysis of foci were performed after irradiation with 1 Gy and examined 1, 6, and 24 hours later, as well as for MNU treatment with 1 mM examined after 1, 6, and 24 hours for the respective cell type. As negative controls, native untreated samples were applied to exclude inherent DNA damage of other origin. As a further control, a second antibody staining was performed (data not shown). For quantification of single foci per cell, fluorescent signals were counted, and the resulting data

are presented as arithmetic means of at least 25 nuclei from at least 2 independent experiments.

Statistical Analysis

The data are presented as arithmetic means with a standard deviation of at least three independent experiments. Two-tailed paired *t* tests were conducted with GraphPad Prism (version 5.01) to determine significance. *p* values lower than .05 were considered as significant (∗, $p = .01–.05$; ∗∗, $p = .001–.01$; ∗∗∗, $p < .001$).

Western Blot Analysis

Total cell extracts were prepared by lysing of an equal number of cells in Roti-Load buffer (Carl Roth GmbH, Karlsruhe, Germany). After heating (95°C, 5 min), 20–30 μg of protein was separated by SDS-polyacrylamide gel electrophoresis (12% gel) and transferred onto nitrocellulose membrane. After blocking (5% nonfat milk in TBS with 0.1% Tween 20; 1 hour at room temperature [RT]), incubation with primary antibodies (1:200–1,000) was performed overnight at 4°C. The activation status of the DDR was analyzed on the levels of phosphorylated kinase ATM (*p*-ATM, Ser1981), histone H2AX (γH2AX, Ser139), checkpoint kinases Chk1 (*p*-Chk1, Ser345) and Chk2 (*p*-Chk2, Thr68), p53 (*p*-p53, Ser15), replication protein RPA32 (*p*-RPA, Ser4/Ser8), and the heterochromatin associated factor Kap1 (*p*-Kap1, Ser824). Phospho-specific antibodies used were obtained from Cell Signaling Technology Inc. (Beverly, MA, http://www.cellsignal.com). After washing with TBS with 0.1% Tween 20, incubation with peroxidase-conjugated secondary antibody (1:2,000; Rockland Immunochemicals Inc., Gilbertsville, PA, http://www.rockland-inc.com) was performed (2 hours at RT). For visualization, the Fusion FX7 imaging system (Peqlab, Erlangen, Germany, http://www.peqlab.com) was used.

RESULTS

Morphology and Dose-Dependent Growth Kinetics in Neonatal and Adult Stromal Cells After Radiation and MNU Treatment

First, the impact of genotoxic treatment was examined by testing several doses ranging from 1 to 15 Gy (for radiation) and from 0.1 to 5 mM (for MNU treatment) for $n = 5$ individual neonatal stromal cell lines and a BM MSC line as an adult counterpart for comparison. Cell counts were determined for at least three passages, and cumulative population doublings were calculated (supplemental online Table 2). Figures in the following section depict representative data from all experiments. Morphology changes were evaluated by assessing the amount of cells revealing apoptotic vesicles and/or detachment of cells.

Radiation

Experiments performed with 1 Gy in neonatal (Fig. 1A) and adult stromal cells (Fig. 1C) revealed a first visible morphological effect after 1 hour in both stromal cell types. With augmenting the dose of radiation up to 3 Gy, more substantial morphological alterations revealing more apoptotic vesicles were observed, but no substantial loss of adherence occurred in either cell type.

Neonatal Stromal Cell Growth Kinetics. Cell counts for this exemplary cell line were determined from passage 5 (P5) to P10, and cumulative population doubling times (CPDs) were calculated. USSCs treated with 1 Gy reached passage 10 after 16 days (CPD 7.36) compared with the untreated control (CPD 10.59). At 2 Gy, passage 9 was reached after 18 days (CPD 5.69), and at 3 Gy it was reached after 17 days (CPD 4.37) (Fig. 1B).

Adult Stromal Cell Growth Kinetics. Cell counts were determined from P6 to P10 for adult stromal cells. Adult BM MSCs revealed a CPD of 6.39 after 13 days in passage 10 (untreated control, 13 days; CPD, 5.82). Treatment with 2 Gy led to a CPD of 2.30 after 13 days in passage 9, and that with 3 Gy led to a CPD of 3.52 (Fig. 1D).

Untreated neonatal stromal cells ($n = 6$ cell lines) revealed a mean CPD per day of 0.59, whereas irradiated cells showed a dose-dependent decrease of CPDs (supplemental online Table 2A). Untreated adult BM MSC controls ($n = 2$) had a lower mean CPD per day (0.35) as compared with neonatal stromal cells because of a lower proliferation rate. Upon irradiation, BM MSCs also revealed a decrease of proliferation rate. However, the proliferation rate according to the 3-Gy treatment was slightly higher as compared with the 2-Gy treatment (Fig. 1D). Both stromal cell types survive the treatment of 1 Gy for more than 14 days, and cell proliferation is hardly affected as compared with the untreated control.

MNU Treatment

First visible morphological effects in both stromal cell types were observed at a concentration of 1 mM MNU (Fig. 1E, 1G). Treatment with MNU promoted more distinct detachment of cells as compared with the untreated control and compared with irradiation. In DMSO controls (solvent of MNU), cells revealed no significant impact either on the adherence of cells or on the morphology.

Neonatal Stromal Cell Growth Kinetics. Cell counts for this exemplary cell line were determined from P6 to P14. Regarding the cumulative population doublings, 1 mM MNU caused a reduction of proliferation in neonatal stromal cells (passage 14; day 38; CPD, 21.17) versus untreated control (passage 14; day 27; CPD, 18.58). At 3 mM MNU, a growth stop occurred in neonatal stromal cells after 13 days in passage 8 (CPD, 1.8) (Fig. 1F).

Adult Stromal Cell Growth Kinetics. Cell counts were determined from P7 to P14 for adult stromal cells. Proliferation of BM MSCs was strongly inhibited after treatment with 1 mM MNU (passage 14; day 34; CPD, 5.95) compared with the untreated control (passage 14; day 45; CPD, 10.33). Growth arrest in BM MSCs was reached with 3 mM MNU after 17 days (passage 11; CPD, 2.37) (Fig. 1H).

Untreated neonatal stromal cells ($n = 4$ cell lines) had a mean CPD per day of 0.56 and showed a dose-dependent decrease upon MNU treatment (supplemental online Table 2B). Neonatal and adult stromal cells revealed a strong impact on proliferation rate after treatment with 3 mM MNU (supplemental online Table 2B).

Taken together, neonatal and adult stromal cell types display similar morphological outcomes after genotoxic stress characterized by no substantial loss of cells, and proliferation capacity was hardly affected at a radiation dose of 1 Gy and a MNU concentration of 1 mM.

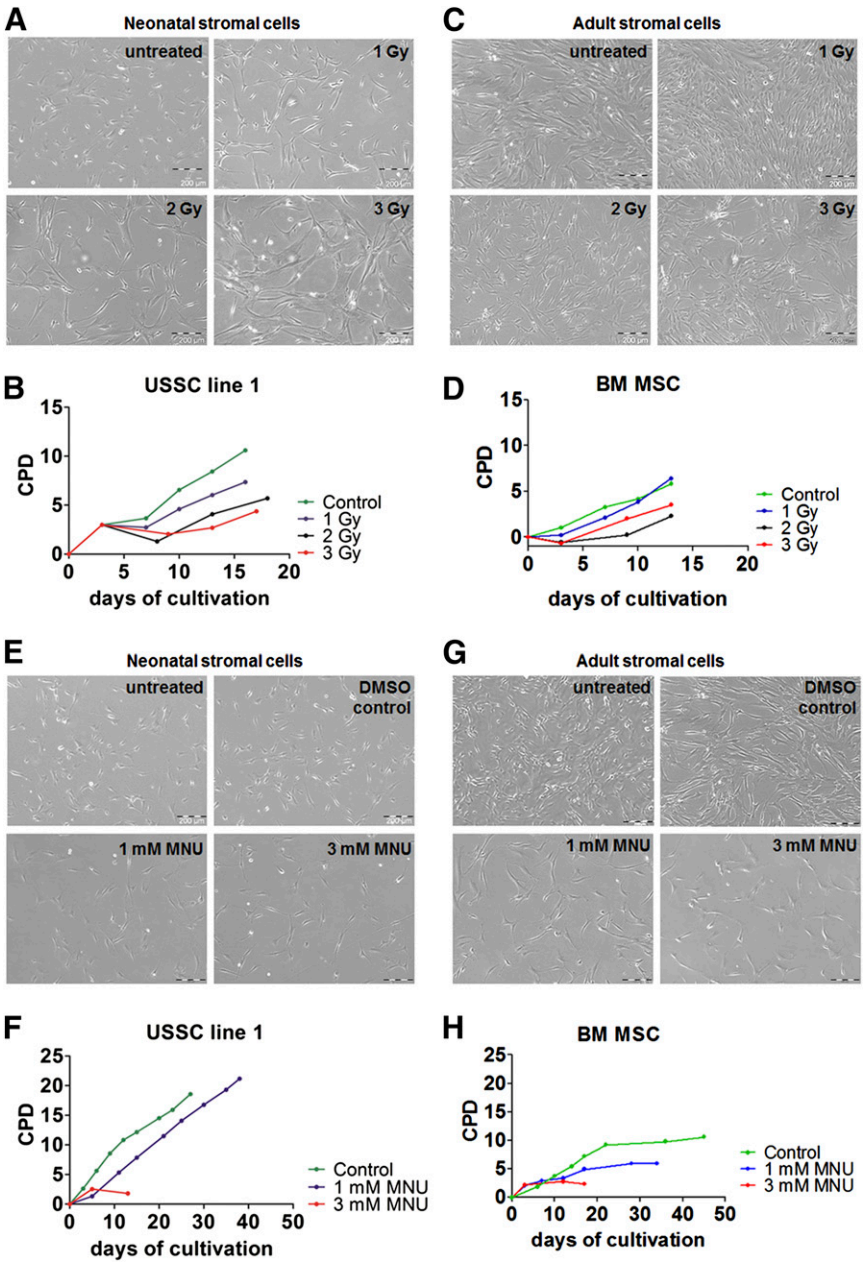

Figure 1. Impact of genotoxic stress on stromal cell morphology and growth. **(A–D):** Dose-dependent effect of radiation on stromal cells. **(A, C):** Representative micrographs of untreated and treated neonatal USSCs and adult BM MSCs irradiated with 1, 2, and 3 Gy. Morphology was analyzed 1 hour later. Scale bars = 200 μm. **(B, D):** Representative growth kinetics. Cells were exposed to different doses of radiation, and long-term growth curves are presented revealing a dose-dependent influence on the proliferation rate of treated cells. The data shown are the CPDs. **(E–H):** Dose-dependent effect of MNU treatment on stromal cells. **(E, G):** Representative micrographs of USSCs and adult BM MSCs and cells treated with 1 and 3 mM MNU. Morphology was analyzed 1 hour later. Scale bars = 200 μm. **(F, H):** Representative growth kinetics. Cells were exposed to several doses of MNU, and long-term growth curves are demonstrated, revealing a dose-dependent influence on the proliferation rate of treated cells. The data shown are the CPDs. Abbreviations: BM MSC, bone marrow multipotent stromal cell; CPD, cumulative population doubling; DMSO, dimethyl sulfoxide; MNU, *N*-methyl-*N*-nitrosurea; USSC, unrestricted somatic stromal cell.

iPSCs Reveal Strong Morphological Effects After Radiation and MNU Treatment

Irradiation and MNU Treatment in iPSCs

The pluripotency status of iPSCs was confirmed on protein level by flow cytometric analysis for stem cell markers SSEA-4, TRA1-60, and TRA1-81, as well as by RT PCR on transcript level for stem cell marker *OCT4A*, *SOX2*, and *NANOG* expression (supplemental online Fig. 1). In order to define whether reprogrammed iPSCs harbor a different susceptibility to DNA damage in comparison with stromal cell types, experiments with colony-forming iPSCs generated from a neonatal USSC line [27] were performed. Effects of radiation and treatment with MNU were analyzed 1, 6, and 24 hours after respective treatment.

Radiation

Untreated iPSCs revealed a typical colony-like morphology with a smooth but irregular contour (Fig. 2A). A dose of 1 Gy

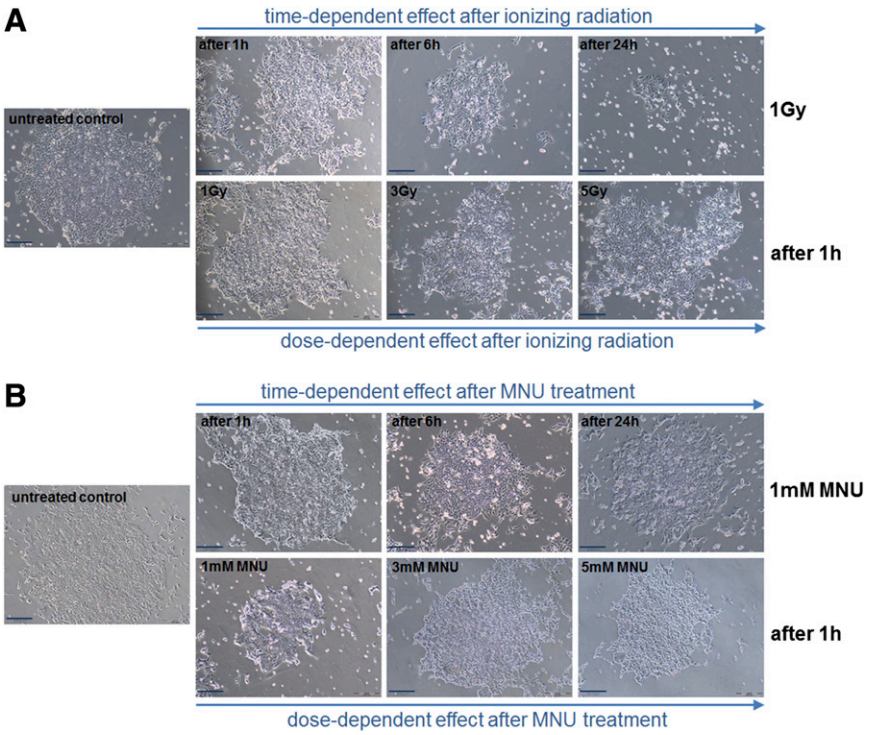

Figure 2. Impact of genotoxic stress on induced pluripotent stem cells (iPSCs) morphology. **(A):** Time- and dose-dependent effect of irradiation on iPSCs. Representative micrographs of irradiated iPSCs are depicted. The cells were exposed to a dose of 1-, 3-, or 5-Gy ionizing radiation, and pictures were taken 1, 6, or 24 hours after treatment. Scale bars = 200 μm. **(B):** Time- and dose-dependent effect of MNU treatment on iPSCs. Representative micrographs of MNU-treated iPSCs are depicted. The cells were exposed to a dose of 1, 3, or 5 mM MNU, and pictures were taken 1, 6, or 24 hours after treatment. Scale bars = 200 μm. Abbreviations: h, hour(s); MNU, *N*-methyl-*N*-nitrosurea.

caused a visible dissolution of the typical iPSC colony already after 1 hour. This dissolution appeared stronger after 6 hours and after 24 hours, whereas smaller compact colonies were detectable. However, at 3 and 5 Gy, more cells lost their adherence, and the iPSC colony changed its typical morphology, indicating dose-dependent cytotoxicity having occurred.

MNU Treatment

iPSCs treated with a concentration of 1 mM MNU had more apoptotic cells as compared with the untreated control, but colony structure was mostly unaffected. After 6 hours, 1 mM of MNU caused a visible dissolution of colonies that was comparable to the samples fixed after 24 hours. Obvious dissolution could be observed in samples treated with 3 and 5 mM MNU, and much less compact colonies were observable. The DMSO controls in iPSCs after 1 and 6 hours were comparable to the untreated control. Of note, treatment with DMSO alone caused loss of colony structure and appearance of apoptotic cells after 24 hours (data not shown) (Fig. 2B).

These results presented here clearly show that iPSCs revealed a much higher sensitivity against MNU, resulting in a loss of colony structure and detachment at lower doses as compared with stromal cell types. Already 0.3 mM MNU caused a first visible detachment of cells and massive loss of colony structure (supplemental online Fig. 2), whereas both stromal cell types showed no substantial loss of adherence. To summarize, iPSCs revealed more pronounced cytotoxicity following genotoxic stress as indicated by substantially stronger morphological alterations after radiation and MNU treatment as compared with neonatal and adult stromal cells.

Foci Analyses of *p*-ATM and γH2AX Revealed Efficient Damage Induction and DNA Repair in iPSCs and Neonatal, and Adult Stromal Cells

In order to detect the direct DNA damage response, the so-called foci analysis was performed. ATM belonging to the superfamily of phosphatidylinositol 3-kinase-related kinases and γH2AX (H2A histone family, member X) are prominent sensors for damage repair. Both phosphorylated proteins can be detected at the DNA location of active damage repair building fluorescent foci [41]. Immunocytochemical staining revealed that the number of γH2AX and *p*-ATM foci per cell was strongly upregulated upon irradiation in iPSCs, neonatal USSCs, and adult BM MSC (Fig. 3A–3D; supplemental online Fig. 3A–3C).

Radiation

Compared with the untreated control, in which single fluorescent foci were rarely detectable, accounting for basal endogenous DNA damage, treatment with 1 Gy lead to the appearance of 29 $\pm$ 6 γH2AX foci per cell (n = 46) 1 hour after irradiation of neonatal stromal cells (Fig. 3B, 3D) versus 23 $\pm$ 8 (n = 85) in iPSC (Fig. 3A, 3D). A significant p value of 0.0051 (**) was determined for USSCs versus iPSCs 1 hour after treatment. BM MSCs had 26$\pm$ 8 γH2AX foci per cell (n = 51) 1 hour after treatment without significant differences to USSCs or iPSCs (Fig. 3C, 3D). At 6 hours after irradiation, most of the cells already had a much lower amount of

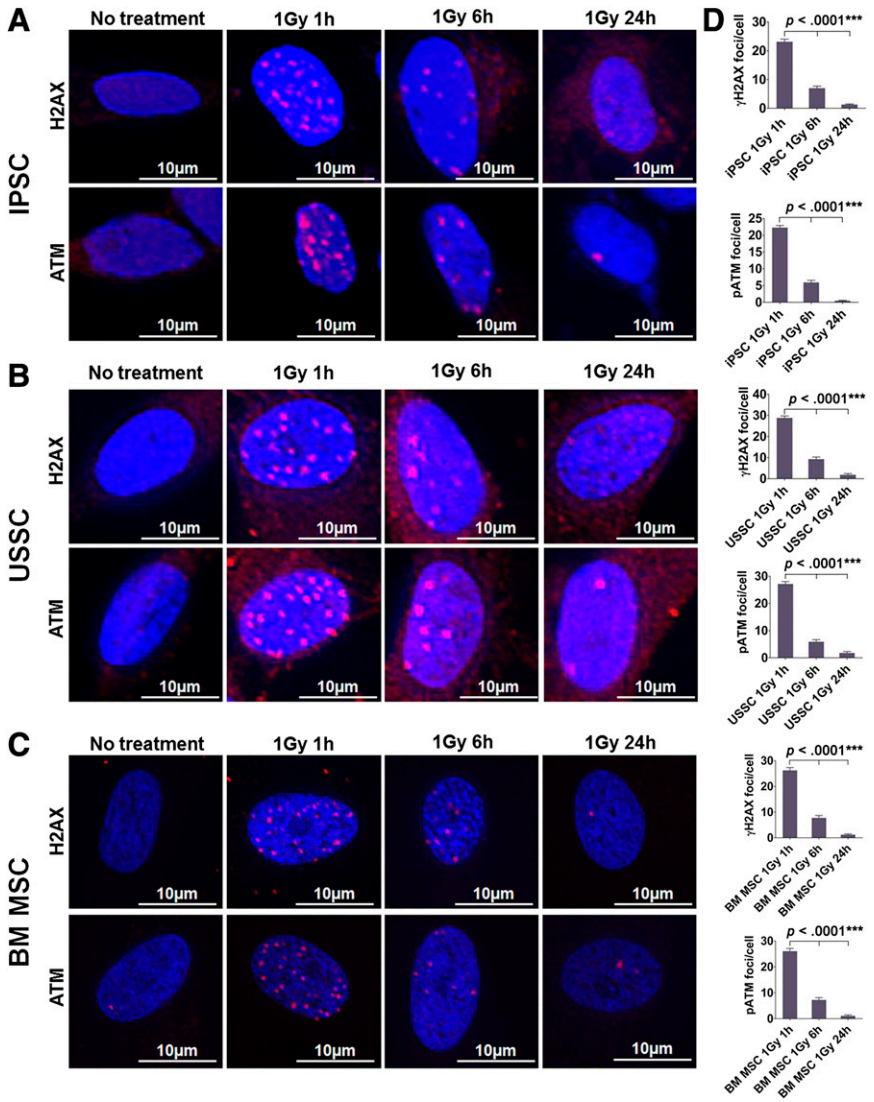

Figure 3. Repair of double-strand breaks in irradiated iPSCs, neonatal stromal cells, and adult BM MSCs. **(A–C):** Representative micrographs for phosphorylated ATM and γH2AX foci in iPSCs **(A)**, neonatal stromal cells **(B)**, and adult BM MSCs **(C)** irradiated with 1 Gy and fixed after 1, 6, and 24 hours of treatment. **(D):** Quantification of single foci representing the mean amount of foci per cell with SD. Two-tailed paired *t* tests were conducted to test significance. Abbreviations: BM MSC, bone marrow multipotent stromal cell; h, hour(s); iPSC or IPSC, induced pluripotent stem cell; USSC, unrestricted somatic stromal cell.

actively repaired DNA locations (USSCs, 9 ± 5 γH2AX foci per cell; *n* = 28 versus iPSC, 7±7 γH2AX foci per cell; *n* = 104 versus BM MSCs, 8 ±7 γH2AX foci per cell; *n* = 58), which was not significantly different between all three cell types. After 24 hours, nearly all cells fully repaired all DNA double-strand breaks (USSCs, 2 ± 3 γH2AX foci per cell; *n* = 40 versus iPSCs, 1 ± 1 γH2AX foci per cell; *n* = 45 versus BM MSCs, 1 ± 2 γH2AX foci per cell; *n* = 58), confirming a successful and effective DNA damage repair finished after 24 hours. Irradiation with 3 and 5 Gy was performed as well after 1 hour (data not shown), revealing a dose-dependent increase of foci, but these foci were hardly countable accurately because of strong overlapping of single foci.

For *p*-ATM, similar amounts of foci were observed in all cell types tested: USSC, 1 Gy 1 hour 27 ± 5 (*n* = 36); 1 Gy 6 hours 6 ± 5 (*n* = 32); 1 Gy 24 hours 2 ±4 (*n* = 61) and BM MSCs, 1 Gy 1 hour 26 ±7 (*n* = 47); 1 Gy 6 hours 7 ± 6 (*n* = 51); 1 Gy 24 hours 1 ± 3 (*n* = 53), revealing similar amounts of foci without any significant differences. After radiation of iPSCs (Fig. 3A, 3D), fewer foci were counted as compared with USSCs (Fig. 3B, 3D): 1 Gy 1 hour 22 ± 5 (*n* = 73); 1 Gy 6 hours 6 ± 5 (*n* = 69); 1 Gy 24 hours 1 ± 1 (*n* = 41). However, the only significant difference of *p*-ATM foci was observed for USSCs versus iPSCs 24 hours after treatment with a *p* value of .0017 (**).

MNU Treatment

In general, an increase of foci was observed after treatment in iPSCs and both stromal cell types in individual cells (supplemental online Fig. 4). However, the number of foci was much more heterogeneous as compared with cells treated with irradiation. Not all cells revealed clear foci, but some of them also showed a strong pan staining. Therefore, a sophisticated quantification of foci was not applicable here. The unequal distribution of foci between single cells and the presence of pan-stained cells

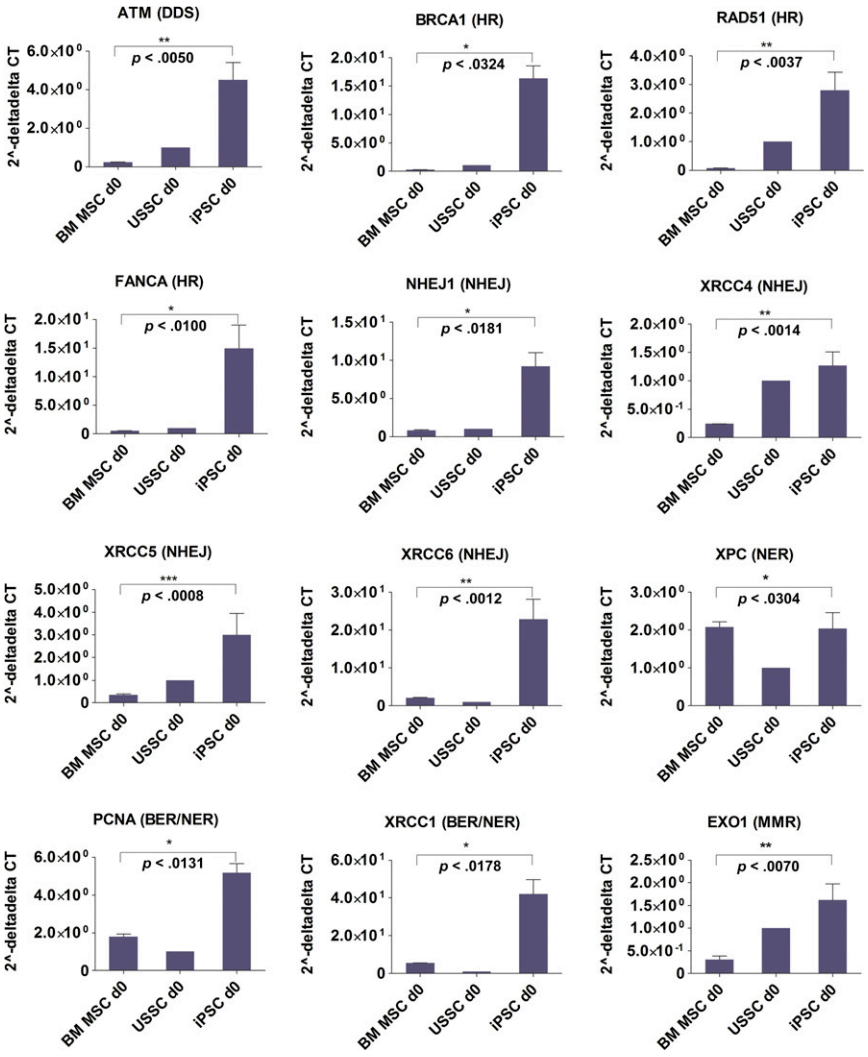

Figure 4. Basic expression level of DNA damage repair genes in stromal cells and iPSCs. Expression of DNA damage repair genes in untreated neonatal stromal cells, adult BM MSCs, and iPSCs is shown. Fold differences in mRNA expression were calculated using the 2^-$\Delta\Delta$CT method relative to neonatal stromal cells and normalized to the reference gene *RPL13A*. According DNA damage response pathways are given in parentheses after the gene name. Abbreviations: BER, base excision repair; BM MSC, bone marrow multipotent stromal cell; d, day; DDS, DNA damage signaling; HR, homologous recombination; iPSC, induced pluripotent stem cell; MMR, mismatch repair; NER, nucleotide excision repair; NHEJ, nonhomologous end-joining; USSC, unrestricted somatic stromal cell.

indicate that MNU-induced damage might vary in a cell cycle-dependent manner. Independent of the time after MNU treatment cells without foci, a high number of foci and pan-stained cells were found (supplemental online Fig. 4A; 1 mM MNU 1 hour iPSCs) in all cell types tested, making an accurate calculation of the repair of alkylation damage impossible.

The Basic Expression Level of DNA Damage Repair Genes Is Higher in iPSCs Compared with Neonatal and Adult Stromal Cell Types

Basic expression level of DNA damage repair genes was analyzed in untreated stromal cell types compared with iPSC by qPCR (Fig. 4). As a typical candidate reflecting DNA damage signaling, the expression of ATM was analyzed. BRCA1 (breast cancer 1 gene), RAD51 (RAD51 homolog *Saccharomyces cerevisiae*), and FANCA (FANCA gene) were chosen as representatives of HR. NHEJ1 (nonhomologous end-joining factor 1) and XRCC4, XRCC5, and XRCC6 (x-ray repair cross-complementing factors 4, 5, and 6) are involved in the NHEJ pathway. Exonuclease 1 (EXO1) is from the MMR pathway. XPC (xeroderma pigmentosum, complementation group C), proliferating cell nuclear antigen (PCNA), and XRCC1 are candidates from the NER and BER pathway.

All damage repair genes tested were upregulated in iPSCs compared with both stromal cell types. IPSCs revealed in comparison with adult BM MSCs a significant upregulation of genes (respective *p* values are presented in Fig. 4).

In addition, adult BM MSC revealed a downregulation in 8 of 12 DDR genes compared with neonatal stromal cells significantly downregulated with a negative fold change less than −2: *RAD51* (−11.81-fold; *p* value < .0001, ***), *BRCA1* (−5.02-fold; *p* value = .0007, ***), *ATM* (−4.70-fold; *p* value = .0006, ***), *EXO1* (−4.2-fold; *p* value < .0001, ***), *XRCC4* (−4.14-fold; *p* value < .0001, ***), and *XRCC5* (−2.77-fold; *p* value = .0067, **). *XRCC6* (2.11-fold; *p* value = .0147, *) and *XRCC1* (5.58-fold; *p* value < .0001, ***) were significantly upregulated compared

with the neonatal counterpart, whereas downregulated *FANCA* (−1.88-fold; *p* value = .0020, **) and *NHEJ* (−1.28-fold; *p* value = .0046, **) and upregulated *XPC* (1.94-fold; *p* value = .0304, *) and *PCNA* (1.76-fold; *p* value < .0001, ***) revealed the lowest fold change differences.

IPSCs in comparison with USSCs also revealed upregulation of respective genes. *XRCC1* was upregulated in iPSCs with the highest fold change of 42.08 (*p* value = .0126, *) compared with neonatal stromal cells. Other (more than twofold) upregulated genes compared with USSCs were: *XRCC6* (22.91-fold; *p* value = .0006, ***), *BRCA1* (16.33-fold; *p* value = .0355, *), *FANCA* (14.93-fold; *p* value = .0104, *), *NHEJ1* (9.24-fold; *p* value = .0191, *), *PCNA* (5.17-fold; *p* value = .0150, *), *ATM* (4.51-fold; *p* value = .0095, **), *XRCC5* (3.01-fold; *p* value = .0018, **), *RAD51* (2.79-fold; *p* value = .0191, *), and *XPC* (2.05-fold; *p* value = .0600, not significant [ns]). Only *EXO1* (1.62-fold; *p* value = .4895, ns) and *XRCC4* (1.27-fold; *p* value = .0416, *) were upregulated with a fold change lower than 2 in iPSCs versus USSCs. Taking these results together, a developmental age-dependent expression of DDR and DNA repair-related genes can be postulated.

Influence of Developmental Age on Mechanisms of the DDR Following Treatment With Ionizing Radiation or the Alkylating Agent MNU

In order to comparatively analyze the DDR of iPSCs, neonatal USSCs, and adult BM MSCs, the cells were irradiated (5 Gy) or treated with the methylating carcinogen MNU (1 mM). After postincubation periods of 1 and 6 hours, the phosphorylation status of key factors of the DDR was determined by Western blot analysis. Following irradiation, a clear increase in the protein level of autophosphorylated ATM was observed in USSCs and BM MSCs (Fig. 5A). This was not observed in iPSC. Moreover, IR stimulated a transient activation of Chk1 (*p*-Chk1) in iPSCs, whereas neonatal and adult stromal cells revealed a prolonged increase in *p*-Chk1 level (Fig. 5A). Activation of Chk2 (*p*-Chk2) occurred in iPSCs, USSCs, and BM MSCs and showed the strongest response in iPSCs. Stimulation of p53 (*p*-p53) was also most prominent in iPSCs after both treatments (Fig. 5A, 5B). As opposed to both stromal cell types, iPSCs revealed a clear activation of replication protein A (*p*-RPA) (Fig. 5A, 5B). Activation of chromatin regulatory factor Kap1 (*p*-Kap1) was observed in USSCs and BM MSCs only after irradiation (Fig. 5A). Taken together, iPSCs showed the most comprehensive activation of DDR mechanisms following treatment with both noxae.

Effect of Irradiation and Treatment With MNU on Osteogenesis Capacity of Neonatal and Adult Stromal Cells

Expression of DDR and Repair Genes During Osteogenesis

The basic expression level of 12 DDR and DNA repair-related genes was analyzed in untreated neonatal stromal cells and adult stromal cells by qPCR during osteogenic differentiation at day 0 (d0), d7, and d14 in *n* = 3 independent experiments. All genes tested (except *XPC*) revealed a significant downregulation (*p* values, ** and ***) at d7 and d14 compared with d0 in USSCs and BM MSCs (Fig. 6). A detailed table of individual fold change differences between d0 versus d7 and d0 versus d14 with respective *p* values is available in supplemental online Table 3. In contrast, *XPC* was upregulated 1.4-fold (*p* value, .1522, ns) in BM MSCs at d0 versus d14. As a result, it can be claimed that the expression of genes that are related to DDR and DNA repair are significantly downregulated during osteogenic differentiation.

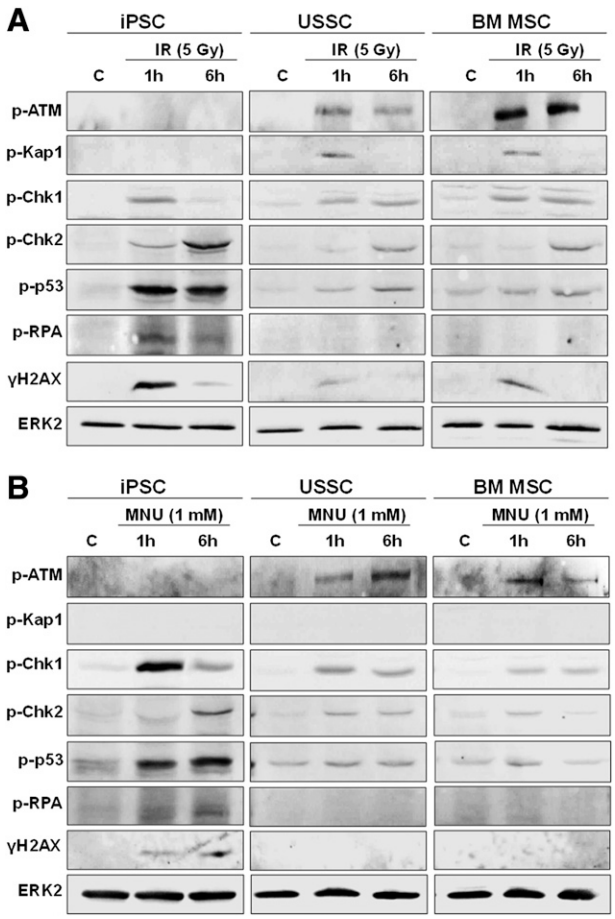

Figure 5. DNA repair activity in stromal cell types compared with iPSCs. **(A, B):** Neonatal USSCs, adult BM MSCs, and iPSCs were irradiated at 5 Gy **(A)** or treated with 1 mM of the methylating carcinogen MNU **(B)**. After postincubation periods of 1 and 6 hours, the phosphorylation status of key factors of the DNA damage response was determined by Western blot analysis. Abbreviations: BM MSC, bone marrow multipotent stromal cell; C, control; h, hour(s); iPSC, induced pluripotent stem cell; IR, ionizing radiation; MNU, *N*-methyl-*N*-nitrosurea; USSC, unrestricted somatic stromal cell.

Impact of Genotoxic Treatment on Osteogenesis

To determine whether treatment with low doses of genotoxins affects the inherent osteogenic potential, neonatal stromal cells and adult stromal cells were damaged either at d0 and afterward cultivated for further 14 days or damaged at d7 of differentiation and afterward cultivated for further 7 days until final readout at day 14. The influence on the osteogenic differentiation potential of neonatal stromal cells in comparison with adult BM MSC was assessed by common alizarin and von Kossa staining, displaying the grade of calcification. Independent from the genotoxic agent used in this experiment, a strong effect was visible in the cells treated at d0 prior to osteogenic differentiation. Alizarin staining after irradiation (USSCs in Fig. 7A, 7C; BM MSCs in Fig. 7E, 7G) revealed a highly significant (*p* value < .0001, ***) lower grade of calcification in neonatal and adult stromal cells damaged at d0 compared

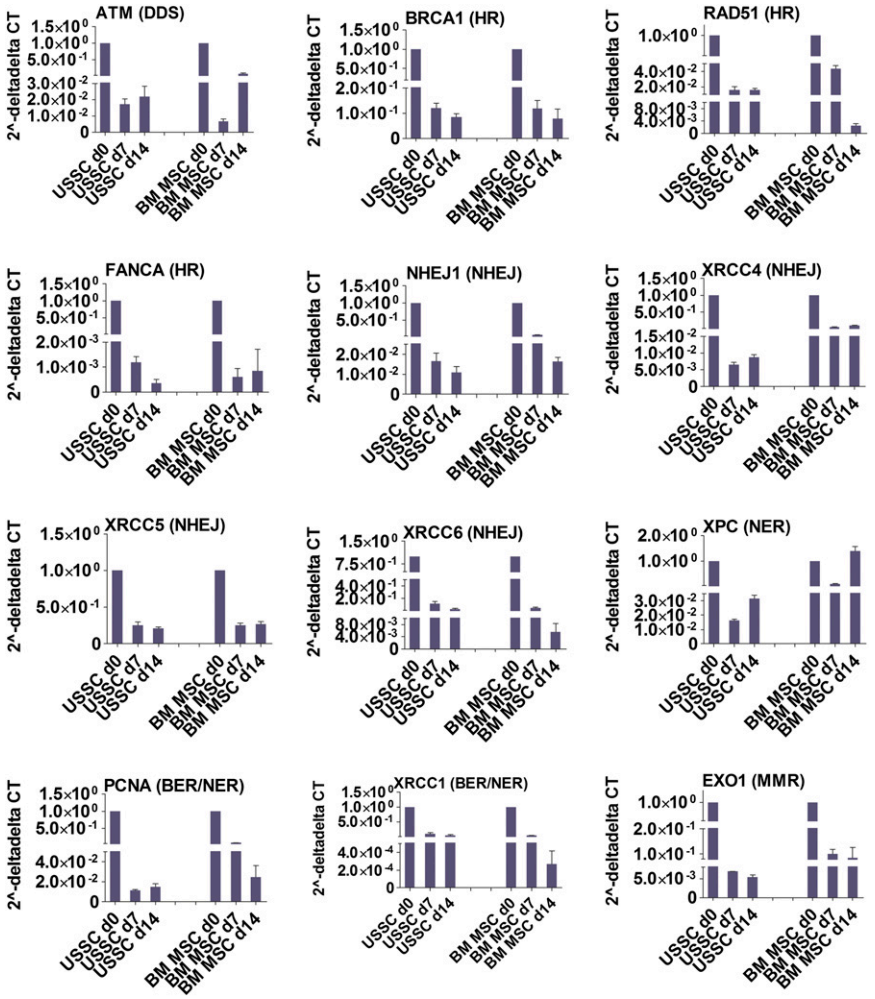

Figure 6. Expression pattern of DNA damage repair genes in neonatal and adult stromal cells during osteogenesis. Expression fold differences were calculated using the 2^-$\Delta\Delta$CT method relative to day 0 samples without osteogenic induction and normalized to the reference gene *RPL13A*. According DNA damage response pathways are given in parentheses after the gene name. Abbreviations: BER, base excision repair; BM MSC, bone marrow multipotent stromal cell; d, day; DDS, DNA damage signaling; HR, homologous recombination; MMR, mismatch repair; NER, nucleotide excision repair; NHEJ, nonhomologous end-joining; USSC, unrestricted somatic stromal cell.

with d7. After treatment with MNU, the most significant difference was observed in samples treated at d0 versus the untreated control (USSCs in Fig. 7D: *p* value = .0007, ***; BM MSCs in Fig. 7H: *p* value = .0090, **). The quantitative analysis of alizarin dye manifests the prior results (USSCs in Fig. 7C, 7D; BM MSCs in Fig. 7G, 7H). For irradiation experiments (Fig. 7C), nonsignificant differences in calcification were found in USSCs irradiated with 1 Gy at d0 (mean relative extinction, 1.4; SD, 0.7) compared with the untreated control (relative extinction, 1.4; SD, 0.1). USSCs treated at d7 (relative extinction, 2.0; SD, 0.8) revealed a significant impact (*p* value = .0256, *) compared with the untreated control. For BM MSCs, no significant influence was detected by alizarin quantification comparing treatment at d7 versus the untreated control for both genotoxic agents. However, treatment of BM MSCs with MNU at d7 revealed a lower visual alizarin staining, which was not reflected by quantification.

Time kinetic analysis (1, 6, and 24 hours) revealed no time-dependent effect on calcification grade of USSCs (supplemental online Fig. 5). Taken together, exposure of cells at d0 turned out to be particularly sensitive to genotoxic stress. In addition, a dose-dependent decrease of calcification was determined in neonatal stromal cells treated with 3 and 5 mM MNU (supplemental online Fig. 6).

Taken together, damage at d0 diminishes the grade of calcification in neonatal and adult stromal cells in a similar way. Interestingly, irradiation at d7 caused an even higher calcification as compared with the untreated control in both stromal cell types, whereas MNU treatment at d7 compared with the control was mainly unaffected.

Discussion

Adequate responses to endogenous or exogenous genotoxic insults are essential for maintenance of genomic integrity and are of particular physiological relevance in the context of development and differentiation. All cells have to cope with damaged DNA, but the sensitivity between distinct cell types at distinct developmental stages is likely variable. Understanding the mechanisms by which stem cells and progenitor cells activate

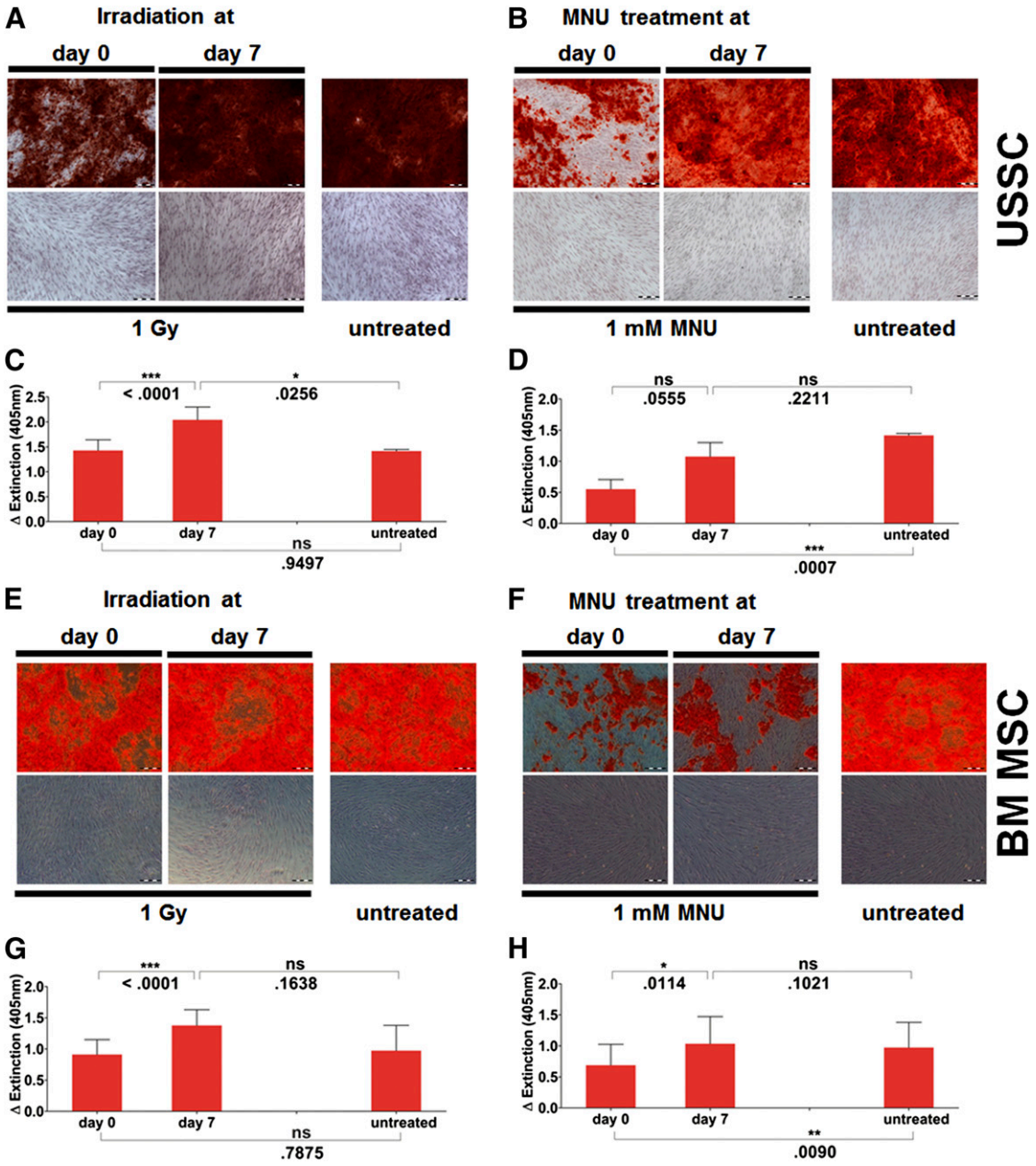

Figure 7. Osteogenic differentiation and alizarin quantification measurement. **(A, B, E, F):** Osteogenic differentiation of neonatal and adult stromal cells after irradiation **(A, E)** and MNU treatment **(B, F)**. Cells were either treated at day 0 or treated at day 14. Alizarin red staining of differentiated cells (upper row) and control cells without induction medium (lower row) is shown. Scale bars = 200 μm. **(C, D, G, H):** Respective alizarin quantification measurement defining the total amount of dye correlating to the grade of calcification. Alizarin quantification was performed $n = 3$ in triplicate for each treatment. The data presented are the mean values of three independent experiments with the same cell line given with standard deviation. Abbreviations: BM MSC, bone marrow multipotent stromal cell; MNU, *N*-methyl-*N*-nitrosurea; ns, not significant; USSC, unrestricted somatic stromal cell.

an effective DDR is also very important if these cells have to realize their full potential in regenerative processes. Therefore, the DNA damage response and repair capacity of neonatal stromal cells was analyzed in comparison with adult stromal cells and USSC-derived iPSC [27].

Genotoxic treatment with either radiation or the alkylating carcinogen MNU revealed a stronger morphological impact on iPSC as compared with stromal cells, pointing to a higher susceptibility of iPSCs to genotoxic stress. This result is in agreement with recently published data of Momcilovic et al. [19], who observed a hypersensitivity to γ-irradiation, followed by substantial detachment of cells after 24 hours, resulting in rapid induction of apoptosis in human iPSCs. Neonatal stromal cells as analyzed here were much more resistant and kept their adherence and morphology at identical doses, suggesting a radioresistance that is comparable to BM MSCs as their adult counterpart [22].

In addition, the basic expression level of DNA damage repair genes was already higher in untreated iPSCs. The lowest basic expression level was determined in adult stromal cells, with a downregulation in 8 of 12 genes tested as compared with their neonatal

counterpart. Therefore, it can be assumed that the expression level of DDR genes is lowest in adult stromal cells, followed by neonatal stromal cells, with iPSCs revealing the highest basic expression level.

In general, stem cells are believed to possess a higher radiosensitivity as compared with more adult cells. However, examples exist of less sensitive murine iPSCs compared with hematopoietic stem/progenitor cells [42]. In the recent work of Nicolay et al. [43], the stem cell characteristics of human BM MSCs after radiation were compared with fibroblast cells. Their study revealed that BM MSCs were not more radiosensitive than human primary fibroblasts and retained their typical stem cell characteristics.

The results described here support the hypothesis that neonatal stromal cells can be regarded as the neonatal counterpart of adult BM MSC, because both stromal cell types revealed a comparable sensitivity to both types of genotoxic stressors. One of the first cellular responses to DNA DSBs is the rapid phosphorylation of histone H2AX by phosphorylated ATM. When DSBs are repaired, H2AX phosphorylation declines with time [44].

In order to define how neonatal stromal cells, adult stromal cells, and iPSCs respond to the induction of DNA damage, foci formation of *p*-ATM and γH2AX was investigated by immunochemistry at different time points to characterize their repair efficiency. Neonatal stromal cells, adult BM MSCs, and iPSCs revealed the strongest increase of nuclear foci 1 hour after irradiation, whereas foci disappeared after 24 hours because of an effective repair reaching the level of the untreated control. In the work of Momcilovic et al. [19], iPSCs reached the steady-state level already after 6 hours postirradiation, but this slight difference might be due to interlaboratory variations and different irradiation procedure. Based on the data, it can be concluded that neonatal stromal cells and iPSCs harbor similar effective DDR mechanisms. iPSCs showed the most comprehensive activation of DDR mechanisms following radiation treatment in Western blot analyses.

Because activation of ATM was not observed in stem cells, we speculate that ATR, which is most important for replicative stress responses [45–47] and has been reported to monitor genomic integrity during neurogenesis [48], is mainly responsible for the regulation of IR-induced DDR mechanisms in proliferating iPSCs. Similar results were obtained following treatment with the methylating agent MNU. Although MNU caused a substantial increase in *p*-ATM levels in USSCs and BM MSCs only, iPSCs revealed a stronger activation of Chk1, Chk2, p53, and RPA as compared with the neonatal and adult cell types. Summarizing, the data disclose substantial differences in the activation of mechanisms of the DDR in human iPSC cells in comparison with neonatal and adult stromal cell types.

Upon osteogenic differentiation, a significant downregulation for all 12 DDR and DNA repair-related genes tested in untreated neonatal stromal cells was observed, which is in agreement with other published data in human embryonic stem cells [49]. Adult BM MSCs revealed a similar pattern as compared with neonatal stromal cells. Of the 12 tested genes, 11 were significantly downregulated upon osteogenic differentiation, supporting the hypothesis that osteogenic differentiation commonly leads to a downregulation of DDR and DNA repair-related genes.

Interestingly, in BM MSCs only the NER-associated factor *XPC* was not downregulated by osteogenic differentiation at d14, suggesting that BM MSCs might consolidate DNA damage processing via the NER pathway upon osteogenesis. However, in most cases of differentiating cells, a decrease in NER activity was found underlining the strong diversity of DNA repair mechanisms within different cell types [50, 51]. This is further supported by recent publications focusing on different DDR capacities depending on the anatomical origin of cells as shown for human BM MSCs [24] and inherent heterogeneity of mouse bulk cultures executing a heterogeneous DDR [52].

Nicolay et al. [43] were able to confirm for human adult MSCs that the inherent osteogenic differentiation potential was not affected after exposure to ionizing radiation. However, an impact on the osteogenic differentiation was observed in our experiments for neonatal stromal cells and adult stromal cells damaged prior to differentiation with 1-Gy irradiation and 1 mM MNU, whereas calcification remained mostly unaffected if damage was induced at d7 of differentiation. Furthermore, treatment with MNU at d0 revealed a dose-dependent reduction of calcification during osteogenesis, suggesting that the response of neonatal stromal cells and adult BM MSCs upon irradiation and MNU treatment is agent-specific. Moreover, our results are strongly supported by the work of Oliver 2013 [53], who revealed a high DNA double-strand break repair activity in undifferentiated human BM MSCs as compared with differentiating osteoblasts revealing apoptosis after irradiation.

It is also well established that fetal bone is exquisitely sensitive to genotoxic stresses during growth of appendicular skeleton, leading to loss of bone mass in adults [54]. This is in line with the data presented in the study at hand showing a reduced osteogenic capacity in human neonatal stromal cells and adult stromal cells.

Conclusion

The results obtained in this study advance the understanding of DNA damage processing in human neonatal stromal cells as compared with adult stromal cells and iPSCs. The data suggest developmental age-dependent differences in DNA damage repair capacity. In iPSCs (closest to embryonic stem cells), the highest expression levels of DDR and repair genes were found, followed by neonatal stromal cells, with adult stromal cells having with the lowest overall expression. In addition, a differentiation-dependent downregulation of repair capacity was observed during osteogenic differentiation in neonatal stromal cells and adult stromal cells. Notably, the impact of genotoxic stress on osteogenic differentiation depends on the time the genotoxic insult takes place and, moreover, is agent-specific. These results strongly support the necessity of offering and establishing adequate cell sources for informative toxicological testing matching to the developmental age and differentiation status of the respective cell of interest.

Acknowledgments

We thank Lara Kern, Lena Schumacher, Ingrid Gelker, and all students involved in this project for their excellent technical support. This work was funded by the German Ministry of Research and Education (Bonn, Germany; Grant BMBF 01 GN 1008D). The project was supported by the Strategischer Forschungsfond

of Heinrich-Heine-University Düsseldorf (GRK 1921 start-up financing).

Author Contributions

S.L.: conception and design, collection and/or assembly of data, data analysis and interpretation, manuscript writing; S.B., D.S., and C.C.: collection and/or assembly of data; T.F.R.: collection and/or assembly of data, data analysis and interpretation; H.Z.: provision of study material; G.F.: conception and design, collection and/or assembly of data, final approval of manuscript; G.K.: conception and design, final approval of manuscript.

Disclosure of Potential Conflicts of Interest

The authors indicated no potential conflicts of interest.

References

1 Shiloh Y. ATM and related protein kinases: Safeguarding genome integrity. Nat Rev Cancer 2003;3:155–168.

2 Harper JW, Elledge SJ. The DNA damage response: Ten years after. Mol Cell 2007;28: 739–745.

3 Kastan MB, Bartek J. Cell-cycle checkpoints and cancer. Nature 2004;432:316–323.

4 Bekker-Jensen S, Mailand N. Assembly and function of DNA double-strand break repair foci in mammalian cells. DNA Repair (Amst) 2010;9: 1219–1228.

5 Woodbine L, Brunton H, Goodarzi AA et al. Endogenously induced DNA double strand breaks arise in heterochromatic DNA regions and require ataxia telangiectasia mutated and Artemis for their repair. Nucleic Acids Res 2011;39:6986–6997.

6 Mahaney BL, Meek K, Lees-Miller SP. Repair of ionizing radiation-induced DNA double-strand breaks by non-homologous end-joining. Biochem J 2009;417:639–650.

7 Hartlerode AJ, Scully R. Mechanisms of double-strand break repair in somatic mammalian cells. Biochem J 2009;423:157–168.

8 Lieber MR. The mechanism of human nonhomologous DNA end joining. J Biol Chem 2008; 283:1–5.

9 Lieber MR, Ma Y, Pannicke U et al. Mechanism and regulation of human non-homologous DNA end-joining. Nat Rev Mol Cell Biol 2003; 4:712–720.

10 Wyatt MD. Advances in understanding the coupling of DNA base modifying enzymes to processes involving base excision repair. Adv Cancer Res 2013;119:63–106.

11 Sedgwick B, Bates PA, Paik J et al. Repair of alkylated DNA: Recent advances. DNA Repair (Amst) 2007;6:429–442.

12 Minca EC, Kowalski D. Replication fork stalling by bulky DNA damage: Localization at active origins and checkpoint modulation. Nucleic Acids Res 2011;39:2610–2623.

13 Taira K, Kaneto S, Nakano K et al. Distinct pathways for repairing mutagenic lesions induced by methylating and ethylating agents. Mutagenesis 2013;28:341–350.

14 Li GM. Mechanisms and functions of DNA mismatch repair. Cell Res 2008;18:85–98.

15 Sherman MH, Bassing CH, Teitell MA. Regulation of cell differentiation by the DNA damage response. Trends Cell Biol 2011;21: 312–319.

16 Nagaria P, Robert C, Rassool FV. DNA double-strand break response in stem cells: Mechanisms to maintain genomic integrity. Biochim Biophys Acta 2013;1830:2345–2353.

17 Fan J, Robert C, Jang YY et al. Human induced pluripotent cells resemble embryonic stem cells demonstrating enhanced levels of DNA repair and efficacy of nonhomologous end-joining. Mutat Res 2011;713:8–17.

18 Lan ML, Acharya MM, Tran KK et al. Characterizing the radioresponse of pluripotent and multipotent human stem cells. PLoS One 2012; 7:e50048.

19 Momcilovic O, Knobloch L, Fornsaglio J et al. DNA damage responses in human induced pluripotent stem cells and embryonic stem cells. PLoS ONE 2010;5:e13410.

20 Momčilović O, Navara C, Schatten G. Cell cycle adaptations and maintenance of genomic integrity in embryonic stem cells and induced pluripotent stem cells. Results Probl Cell Differ 2011;53:415–458.

21 Chen MF, Lin CT, Chen WC et al. The sensitivity of human mesenchymal stem cells to ionizing radiation. Int J Radiat Oncol Biol Phys 2006;66:244–253.

22 Sugrue T, Lowndes NF, Ceredig R. Mesenchymal stromal cells: Radio-resistant members of the bone marrow. Immunol Cell Biol 2013;91: 5–11.

23 Prendergast AM, Cruet-Hennequart S, Shaw G et al. Activation of DNA damage response pathways in human mesenchymal stem cells exposed to cisplatin or γ-irradiation. Cell Cycle 2011;10:3768–3777.

24 Damek-Poprawa M, Stefanik D, Levin LM et al. Human bone marrow stromal cells display variable anatomic site-dependent response and recovery from irradiation. Arch Oral Biol 2010; 55:358–364.

25 Rocha CR, Lerner LK, Okamoto OK et al. The role of DNA repair in the pluripotency and differentiation of human stem cells. Mutat Res 2013;752:25–35.

26 Stambrook PJ, Tichy ED. Preservation of genomic integrity in mouse embryonic stem cells. Adv Exp Med Biol 2010;695:59–75.

27 Zaehres H, Kogler G, Arauzo-Bravo MJ et al. Induction of pluripotency in human cord blood unrestricted somatic stem cells. Exp Hematol 2010;38:809–818.

28 Kogler G, Sensken S, Airey JA et al. A new human somatic stem cell from placental cord blood with intrinsic pluripotent differentiation potential. J Exp Med 2004;200: 123–135.

29 Kogler G, Critser P, Trapp T et al. Future of cord blood for non-oncology uses. Bone Marrow Transplant 2009;44:683–697.

30 Kluth SM, Buchheiser A, Houben AP et al. DLK-1 as a marker to distinguish unrestricted somatic stem cells and mesenchymal stromal cells in cord blood. Stem Cells Dev 2010;19:1471–1483.

31 Kluth SM, Radke TF, Kogler G. Potential application of cord blood-derived stromal cells in cellular therapy and regenerative medicine. J Blood Transfus 2012;2012:365182.

32 Liedtke S, Buchheiser A, Bosch J et al. The HOX Code as a "biological fingerprint" to distinguish functionally distinct stem cell populations derived from cord blood. Stem Cell Res (Amst) 2010;5:40–50.

33 Liedtke S, Freytag EM, Bosch J et al. Neonatal mesenchymal-like cells adapt to surrounding cells. Stem Cell Res (Amst) 2013;11: 634–646.

34 Bosch J, Houben AP, Hennicke T et al. Comparing the gene expression profile of stromal cells from human cord blood and bone marrow: Lack of the typical "bone" signature in cord blood cells. Stem Cells Int 2013;2013:631984.

35 Bosch J, Houben AP, Radke TF et al. Distinct differentiation potential of "MSC" derived from cord blood and umbilical cord: Are cord-derived cells true mesenchymal stromal cells? Stem Cells Dev 2012;21:1977–1988.

36 Kluth SM, Radke TF, Kogler G. Increased haematopoietic supportive function of USSC from umbilical cord blood compared to CB MSC and possible role of DLK-1. Stem Cells Int 2013;2013:985285.

37 Sogorb MA, Pamies D, de Lapuente J et al. An integrated approach for detecting embryotoxicity and developmental toxicity of environmental contaminants using in vitro alternative methods. Toxicol Lett 2014;230: 356–367.

38 Aikawa N, Kunisato A, Nagao K et al. Detection of thalidomide embryotoxicity by in vitro embryotoxicity testing based on human iPS cells. J Pharmacol Sci 2014;124:201–207.

39 Piersma AH, Ezendam J, Luijten M et al. A critical appraisal of the process of regulatory implementation of novel in vivo and in vitro methods for chemical hazard and risk assessment. Crit Rev Toxicol 2014;44:876–894.

40 Takahashi K, Tanabe K, Ohnuki M et al. Induction of pluripotent stem cells from adult human fibroblasts by defined factors. Cell 2007; 131:861–872.

41 Bakkenist CJ, Kastan MB. DNA damage activates ATM through intermolecular autophosphorylation and dimer dissociation. Nature 2003;421:499–506.

42 Hayashi N, Monzen S, Ito K et al. Effects of ionizing radiation on proliferation and differentiation of mouse induced pluripotent stem cells. J Radiat Res (Tokyo) 2012;53:195–201.

43 Nicolay NH, Sommer E, Lopez R et al. Mesenchymal stem cells retain their defining stem cell characteristics after exposure to ionizing radiation. Int J Radiat Oncol Biol Phys 2013; 87:1171–1178.

44 Rogakou EP, Pilch DR, Orr AH et al. DNA double-stranded breaks induce histone H2AX phosphorylation on serine 139. J Biol Chem 1998;273:5858–5868.

45 Cortez D, Guntuku S, Qin J et al. ATR and ATRIP: Partners in checkpoint signaling. Science 2001;294:1713–1716.

46 Mordes DA, Glick GG, Zhao R et al. TopBP1 activates ATR through ATRIP and a PIKK regulatory domain. Genes Dev 2008;22:1478–1489.

47 Paulsen RD, Cimprich KA. The ATR pathway: Fine-tuning the fork. DNA Repair (Amst) 2007;6:953–966.

48 Lee Y, Shull ER, Frappart PO et al. ATR maintains select progenitors during nervous system development. EMBO J 2012;31:1177–1189.

49 Saretzki G, Walter T, Atkinson S et al. Downregulation of multiple stress defense mechanisms during differentiation of human embryonic stem cells. STEM CELLS 2008;26:455–464.

50 Nouspikel T. DNA repair in differentiated cells: Some new answers to old questions. Neuroscience 2007;145:1213–1221.

51 Aoki Y, Sato A, Mizutani S et al. Hematopoietic myeloid cell differentiation diminishes nucleotide excision repair. Int J Hematol 2014; 100:260–265.

52 Sugrue T, Brown JA, Lowndes NF et al. Multiple facets of the DNA damage response contribute to the radioresistance of mouse mesenchymal stromal cell lines. STEM CELLS 2013;31:137–145.

53 Oliver L, Hue E, Séry Q et al. Differentiation-related response to DNA breaks in human mesenchymal stem cells. STEM CELLS 2013;31:800–807.

54 Cooper C, Westlake S, Harvey N et al. Review: Developmental origins of osteoporotic fracture. Osteoporos Int 2006;17:337–347.

See www.StemCellsTM.com for supporting information available online.